

# A simple model of the reflection effect for the interacting binaries and extrasolar planets

J. Budaj

*Astronomical Institute, Slovak Academy of Sciences, Tatranská Lomnica 05960, Slovak Republic*  
budaj@ta3.sk

## ABSTRACT

Extrasolar planets are a natural extension of the interacting binaries towards the companions with very small masses and similar tools might be used to study them. Unfortunately, the generally accepted treatment of the reflection effect in interacting binaries is not very suitable to study cold objects irradiated by hot objects or extrasolar planets.

The aim of this paper is to develop a simple model of the reflection effect which could be easily incorporated into the present codes for modeling of interacting binaries so that they can be used to study above mentioned objects.

Our simple model of the reflection effect takes into account the reflection (scattering), heating and heat redistribution over the surface of the irradiated object. The shape of the objects is described by the Roche potential and limb and gravity darkening can be taken into account. The orbital revolution and rotation of the planet with proper Doppler shifts for the scattered and thermal radiation are also accounted for. Subsequently, light-curves and/or spectra of exoplanets were modeled and the effects of the heat redistribution, limb darkening/brightening, (non-)grey albedo, and non-spherical shape were studied. Recent observations of HD189733b, WASP12b, and Wasp-19b were reproduced reasonably well. HD189733b has low Bond albedo and intense heat redistribution. Wasp-19b has low Bond albedo and low heat redistribution.

We also calculate the exact Roche shapes and temperature distribution over the surface of all 78 transiting extrasolar planets known so far. It is found that the departures from the sphere vary considerably within the sample. Departures of about 1% are common. In some cases (WASP-12b, WASP-19b, WASP-33b) departures can reach about 14, 12, and 8%, respectively. The mean temperatures of these planets also vary considerably from 300 K to 2600 K. The extreme cases are WASP-33b, WASP-12b, and WASP-18b with mean temperatures of about 2600, 2430, and 2330 K, respectively.

*Subject headings:* (stars:) binaries (including multiple): close — (stars:) binaries: eclipsing — stars: low-mass, brown dwarfs — (stars:) planetary systems

## 1. Introduction

There are sophisticated computer codes for calculating and inverting light curves or spectra of binary stars with various shapes or geometry including the Roche model (Lucy 1968; Wilson & Devinney 1971; Wood 1971; Mochnacki & Dougherty 1972; Rucinski 1973; Hill 1979; Popper & Etzel 1981; Zhang et al. 1986; Djurasevic 1992; Drechsel et al. 1994; Linnell & Hubeny 1996; Hadrava 1997;

Orosz & Hauschildt 2000; Bradstreet & Steelman 2002; Pribulla 2004; Pavlovski et al. 2006; Tamuz et al. 2006). The Wilson & Devinney (WD) code is most often used and is continuously being improved or modified (Kallrath et al. 1998; Prša & Zwitter 2005). The reflection effect is taken into account in most of these codes.

The standard description of this effect is given in Wilson (1990). This effect is understood in the following way: A surface element of star A is irra-

diated by many surface elements of star B. A fraction of impinging energy called bolometric albedo (Rucinski 1969) is converted into the heat which rises the local temperature and re-radiates the energy on the day side of the object. Rest of the impinging energy is plunged into the star. Typically, bolometric albedo is set to 1 for radiative and 0.5 for convective envelopes. An increase of the temperature on the day side of one object triggers a secondary reflection effect on the second object and one, two or several iterations are allowed to converge to a final state. Roche model, limb darkening and gravity darkening are taken into account. This model does a good job for many interacting binaries.

However, I argue that the above mentioned model of the reflection effect should be revisited. There has been a lot of progress in the field since the time this reflection effect was developed. New types of very cool objects such as brown dwarfs and extrasolar planets have been discovered. These new areas evolve rapidly and produce interesting results. In many respects, an extrasolar planet can be understood as an interacting binary with a small mass companion. It is thus an attractive idea to apply these new results from the extrasolar planets to interacting binaries and vice versa. For example, models of extrasolar planets can provide day-night heat redistribution and reflected light while models of interacting binaries can provide sophisticated Roche geometry.

The standard model of the reflection effect faces several problems which prevent its application to cool objects irradiated by hot objects and to extrasolar planets. When it comes to very cold strongly irradiated objects a considerable amount of energy might be reflected off the surface. The above mentioned reflection effect in the interacting binaries neglects this reflected light which can be essential, especially at the shorter wavelength. Well known example of such effect are the planets and moons in our Solar system in the visible light. This reflected light bears the spectroscopic signatures of the hot irradiating star and is not converted into the heat and re-radiated. It is commonly taken into account in models of hot-Jupiters or planets in general (Seager et al. 2000; Sudarsky et al. 2005). The definition of the albedo in the planetary sciences is almost the opposite of its meaning in the interacting binaries. In planets, the albedo is a

fraction of the impinging energy which is reflected off the object and is not absorbed and converted into the heat. Reflected and re-radiated photons may also have completely different Doppler shifts depending on the mutual velocities of the two objects and observer.

Moreover, some portion of the energy absorbed on the day side can be transferred to and irradiated from the night side. Various authors developed different parametrization of this effect in connection with the extrasolar planets (Guillot et al. 1996; Burrows et al. 2006; Cowan & Agol 2010). Calculations of atmosphere models of extrasolar planets (Hubeny et al. 2003; Barman et al. 2005; Burrows et al. 2008; Fortney et al. 2008) demonstrate that there is a deep temperature plateau which turns off the convection in the atmospheres. Convection and vertical energy transport operates only at very deep layers. Observations of hot-Jupiters indicate that only a very small fraction of the impinging radiation ( $10^{-4}$ ) could have been plunged into the object (Burrows et al. 2007). Hydrodynamical simulations (Dobbs-Dixon & Lin 2008; Showman et al. 2009; Menou & Rauscher 2009) of the atmospheres of extrasolar planets indicate that there are very strong horizontal currents and jets which can effectively redistribute and circulate the energy between the day and night side of the planet especially along the lines of constant latitudes. How much energy gets redistributed to the night side depends mainly on the complex structure and dynamics of the surface layers.

The above mentioned effects and findings must be taken into account in the new or revisited model of the reflection effect when modeling very cold components of interacting binaries and extrasolar planets. At the same time, many transiting exoplanets are so close to their host stars that their shape may depart from the sphere and be best described by the Roche model.

The main purpose of this paper is to develop a new simple model of the reflection effect which would consider the reflected (scattered) light, heating (absorption of the light), and heat redistribution over the surface and which could be used to model the cold components of interacting binaries and extrasolar planets. The model was included into our code SHELLSPEC (Budaj & Richards 2004; Budaj et al. 2005). This program was origi-

nally designed to calculate light-curves, spectra and images of interacting binaries immersed in a moving circumstellar environment which is optically thin. The code is freely available at <http://www.ta3.sk/~budaj/shellspec.html> and might be used to study various effects observed or expected in the interacting binaries or extrasolar planets. A Fortran90 version of the code which also solves the inverse problem was created by Tkachenko et al. (2010).

## 2. Roche model

In the SHELLSPEC code the Roche model serves as a boundary condition for the radiative transfer in the circumstellar matter. Both objects, star and companion, may have shapes according to the Roche model for detached or contact systems. Descriptions of the Roche model can be found in Kopal (1959), Plavec & Kratochvil (1964), and many other papers and books. Let us assume a Cartesian coordinate system (x,y,z) centered on one of the stars (labeled as 1) such that the companion (labeled as 2) is at (1,0,0) and revolves around the z axis in the direction of positive y axis. Let the mass ratio,  $q$ , always be  $m_2/m_1$  or ‘companion/star’ and  $q < 1$  will indicate the companion is lighter while  $q > 1$  means the central star is lighter. Then, the normalized Roche potential,  $C$ , is expressed as:

$$C(x, y, z) = \frac{2}{(1+q)r_1} + \frac{2q}{(1+q)r_2} + \left(x - \frac{q}{1+q}\right)^2 + y^2 \quad (1)$$

where

$$\begin{aligned} r_1 &= \sqrt{x^2 + y^2 + z^2} \\ r_2 &= \sqrt{(x-1)^2 + y^2 + z^2}. \end{aligned} \quad (2)$$

The Roche surface of a detached component is defined as an equipotential surface  $C_s = C(x_s, y_s, z_s)$  passing through the sub-stellar point  $(x_s, y_s, z_s)$  (point on the surface of the star in between the stars,  $0 < x_s < 1, y_s = z_s = 0$ ) which is localized by the ‘fill-in’ parameter  $f_i \leq 1$ . We define this by:

$$f_i = x_s/L_{1x}, \quad f_i = (1 - x_s)/(1 - L_{1x}) \quad (3)$$

for the primary and the secondary, respectively.  $L_{1x}$  is the x coordinate of the L1 point  $L1(L_{1x}, 0, 0)$ .

Derivatives of the Roche potential are:

$$C_x = \frac{\partial C}{\partial x}, \quad C_y = \frac{\partial C}{\partial y}, \quad C_z = \frac{\partial C}{\partial z} \quad (4)$$

Gravity darkening of the non spherical objects is taken into account by varying the surface temperature according to the von Zeipel’s law:

$$T/T_p = (g/g_p)^\beta \quad (5)$$

where  $g$  is the normalized surface gravity,  $\beta$  is the gravity darkening coefficient,  $T_p, g_p$  are the temperature and gravity at the rotation pole. The normalized gravity vector is  $\mathbf{g} = (C_x, C_y, C_z)$  and:

$$g = \sqrt{C_x^2 + C_y^2 + C_z^2}. \quad (6)$$

Notice, that there is an imminent singularity in the calculations in the vicinity of L1, L2 points since gravity falls to zero which drags temperatures (a denominator in many equations) to zero. We avoid the problem by setting the lowest possible value of  $g/g_p = 10^{-4}$ .

Limb darkening is taken into account using the quadratic limb darkening law:

$$I(\theta) = I(0)f_{LD} \quad (7)$$

$$f_{LD} = 1 - u_1(1 - \cos \theta) - u_2(1 - \cos \theta)^2 \quad (8)$$

and by calculating the cosine of the angle  $\theta$  between the line of sight unit vector  $\mathbf{n} = (n_x, n_y, n_z)$  and a normal to the surface:

$$\cos \theta = -\mathbf{n} \cdot \mathbf{g} / g = -\frac{n_x C_x + n_y C_y + n_z C_z}{\sqrt{C_x^2 + C_y^2 + C_z^2}}. \quad (9)$$

## 3. Irradiation and heat redistribution

In this section we will describe our treatment of the mutual irradiation of the objects. It can be applied to both objects but we will neglect multiple reflections between the two objects since this is not essential if one of them is much less luminous. We will distinguish between three separate processes: **reflection** of the light off the object (or scattering which does not produce any heating of the irradiated surface); **heating** of the irradiated surface (day side) by the absorbed light; and subsequent **heat redistribution** over the entire surface of the object. Let’s assume that the day

side of a planet is irradiated by the star then the impinging flux at a location  $\mathbf{r}$  from star at  $\mathbf{r}_*$  is:

$$F_{ir} = \cos \delta \frac{R_*^2}{(\mathbf{r} - \mathbf{r}_*)^2} \sigma T_*^4 \quad (10)$$

where  $R_*$ ,  $T_*$  are radius and effective temperature of the star,  $\delta$  is an irradiating angle which is the zenith distance of the center of the star as seen from the surface of the planet:

$$\cos \delta = \frac{(\mathbf{r} - \mathbf{r}_*) \cdot \mathbf{g}}{|\mathbf{r} - \mathbf{r}_*| g} = \frac{(r_x - r_{x*})C_x + (r_y - r_{y*})C_y + (r_z - r_{z*})C_z}{|\mathbf{r} - \mathbf{r}_*| \sqrt{C_x^2 + C_y^2 + C_z^2}}. \quad (11)$$

Now, let's define two local parameters  $A_B(\alpha, \beta)$ ,  $P_r(\alpha, \beta)$  on the day side of the planet (irradiated side of an object) where  $\alpha, \beta$  are the longitude and latitude, respectively, measured from the sub-stellar point.  $P_r$  will be the local heat redistribution parameter and  $A_B$  will be the local Bond albedo of the surface. Consequently  $A_B F_{ir}$  is flux immediately reflected off the surface,  $(1 - A_B) F_{ir}$  will be a fraction of the irradiating energy which is converted into the heat,  $P_r(1 - A_B) F_{ir}$  will be a part of the latter which is redistributed over the day and night side of the object, while the remaining part,  $(1 - P_r)(1 - A_B) F_{ir}$ , will heat the local area.<sup>1</sup> Then the energy conservation for the day-night heat transport can be written as:

$$\iint P_r(1 - A_B) F_{ir} dS_{day} = \iint \sigma T_{dn}^4 dS_{day+night} \quad (12)$$

Let's assume, of simplicity (or in the absence of a better approximation), that  $A_B(\alpha, \beta)$ ,  $P_r(\alpha, \beta)$  are constant and the heat is homogeneously redistributed over the day and night sides so that the surface has a constant temperature  $T_0$ . Then,

$$P_r(1 - A_B) \iint F_{ir} dS_{day} / \iint dS_{day+night} = \sigma T_0^4. \quad (13)$$

<sup>1</sup>Note that our local  $P_r$  should not be confused with the global  $P_n$  parameter of Burrows et al. (2006).  $P_n$  is a fraction of the impinging stellar radiation which is transferred to and reradiated from the night side,  $P_n \approx P_r(1 - A_B)/2$ .  $P_n$  is from the interval 0-0.5 while  $P_r$  runs from 0 to 1.  $P_r$  is a direct indicator of the heat redistribution while the  $P_n$  parameter only reflects a combination of the heat redistribution and Bond albedo.

In case the planet has a spherical shape and is far from the star this reduces to:

$$T_0^4 = \frac{1}{4} P_r (1 - A_B) \frac{R_*^2}{d^2} T_*^4. \quad (14)$$

Let's explore another case, namely that the horizontal circulation on the planet along the lines of constant latitude is so strong that it dominates the day-night heat transport and the equilibrium surface temperature,  $T_1$ , will be a function of latitude. In this case and the assumptions above (spherical planet far from the star), one can consider an energy conservation for a fixed latitude:

$$P_r(1 - A_B) \int F_{ir} \cos(\beta) d\alpha = \sigma T_1^4(\beta) \int \cos(\beta) d\alpha \quad (15)$$

where

$$\cos(\delta) = \cos(\alpha) \cos(\beta). \quad (16)$$

The solution is that the temperature depends on the fourth root of  $\cos(\beta)$ :

$$T_1^4(\beta) = \frac{1}{\pi} P_r (1 - A_B) \frac{R_*^2}{d^2} T_*^4 \cos(\beta) = \frac{4}{\pi} T_0^4 \cos(\beta). \quad (17)$$

The study of these two extreme cases lead us to suggest a heat redistribution model in which the day-night heat transport is a linear combination of the two cases mentioned above. Namely, we will express the surface temperature in the following way:

$$T_{dn}^4(\beta) = T_0^4 [P_a + P_b \cos(\beta)] \quad (18)$$

where  $P_a, P_b$  are the 'zonal temperature redistribution parameters'.  $P_a = < 0, 1 >$  and  $P_b$  is to be determined from Eq.12 so that the total energy budget is conserved. From Eq. 12,13 and 18 we obtain:

$$P_b = (1 - P_a) \frac{\iint dS_{day+night}}{\iint \cos \beta dS_{day+night}}. \quad (19)$$

It can be shown that in case of a spherical planet far from the star

$$P_b = \frac{4}{\pi} (1 - P_a) \quad (20)$$

and  $P_b = < 0, 4/\pi >$ . Notice, that  $P_a$  is a measure of the effectiveness of the homogeneous temperature distribution over the surface versus the zonal distribution. It is intimately linked with the effectiveness of the heat flows along the meridians versus parallels.

Finally, the temperature distribution on the surface of the irradiated planet will be:

$$T^4 = T_{ir}^4 + T_{dn}^4 + T_{old}^4 \quad (21)$$

where  $T_{ir}^4 = (1 - P_r)(1 - A_B)F_{ir}/\sigma$  on the day side,  $T_{ir}^4 = 0$  on the night side, and  $T_{old}$  is the prior temperature distribution over the surface in the absence of the irradiation (including the gravity darkening etc.). It should be noted that imposing the external irradiation on one side of the object can alter the original temperature distribution. Budaj et al. (2009) argue that the core cooling rates ( $T_{old}$ ) from the day and night side of a strongly irradiated planet may not be the same and that the difference depends on several important parameters, such as the effectiveness and the depth where the day-night heat transport occurs, the stellar irradiation flux, and vertical redistribution of the opacities, atmospheric abundances, and/or presence of the stratospheres.

Once we know the temperature distribution over the surface, one can approximate the monochromatic flux from the surface as being composed of two parts:

$$F_\nu = F_\nu^{reflect} + F_\nu^{thermal} \quad (22)$$

Reflection depends on the surface albedo  $A_\nu$  and has to take into account the mutual velocities:

$$F_\nu^{reflect} = A_{\nu_2} F_{\nu_1 ir} \quad (23)$$

$$F_{\nu_1 ir} = \cos \delta \frac{R_\star^2}{(\mathbf{r} - \mathbf{r}_\star)^2} F_{\nu_1}^\star \quad (24)$$

where  $F_{\nu_1}^\star$  is properly shifted flux emerging from the surface of the irradiating star. The Doppler shifts are the following

$$\nu_2 = \nu \left(1 - \frac{v_z}{c}\right) \quad (25)$$

$$\nu_1 = \nu \left(1 - \frac{v_z + v_2}{c}\right) \quad (26)$$

$$v_2 = -\frac{(\mathbf{r} - \mathbf{r}_\star) \cdot (\mathbf{v} - \mathbf{v}_\star)}{|\mathbf{r} - \mathbf{r}_\star|} \quad (27)$$

where  $\mathbf{v}$  is the velocity field vector at the given point on the irradiated surface specified by the vector  $\mathbf{r}$ ,  $\mathbf{v}_\star$  is the velocity of the center of mass of the irradiating star, and  $z$  coordinate points to

the observer.<sup>2</sup> To calculate the reflected intensity we assume that the reflection is isotropic in which case:

$$I_\nu^{reflect} = F_\nu^{reflect} / \pi. \quad (28)$$

Finally,  $F_\nu^{thermal}$  can be approximated by the flux emerging from the non-irradiated model atmosphere with the effective temperature equal to the surface temperature of the irradiated object given by Eq.21.

$$F_\nu^{thermal} = F_{\nu_2}(T_{eff} = T) \quad (29)$$

and the associated intensity is given by:

$$I_\nu^{thermal} = I_\nu(0)^{thermal} f_{LD} \quad (30)$$

$$I_\nu(0)^{thermal} = \frac{F_\nu^{thermal}}{\pi(1 - u_1/3 - u_2/6)} \quad (31)$$

In this way we fully include into account the mutual velocities of the objects and observer, the rotation of the reflecting object, its limb darkening but neglect the rotation of the irradiating object. In some cases the later can be easily taken into account by feeding the code with the precalculated rotationally broadened spectrum  $F_\nu^\star$ .

Local Bond albedo used here is a weighted monochromatic albedo  $A_\nu$ :

$$A_B = \frac{\int A_\nu F_\nu^\star d\nu}{\int F_\nu^\star d\nu}. \quad (32)$$

One has to keep in mind that our albedo refers to the reflected light only (not to the absorbed and re-radiated light). In case the irradiated object is very cold compared to the irradiating object there is a clear distinction between its thermal radiation and reflected radiation. However, if the two objects have comparable temperatures it is almost impossible to distinguish whether a particular photon was scattered or absorbed and re-radiated. In this case it is still possible to use our formalism and e.g. approximate the albedo by the single scattering albedo to cope with the problem.

<sup>2</sup>Note that generally Doppler shifts in the scattered and thermal radiation are not the same and may not be trivial. More detailed treatment would require high resolution radiative transfer in the irradiated atmospheres for a set of radial planet-star velocities.

It might be convenient to define the mean temperature of the whole distorted object:

$$T_{mean}^4 \equiv \frac{\int T^4 dS}{\int dS}. \quad (33)$$

Note that it does not take into account the reflected light and should not be confused with the effective temperature or brightness temperature.

#### 4. Application to extrasolar planets

Extrasolar planets are an attractive test-bed for such models. They are a natural extension of the interacting binaries towards cool and small mass companions. Their radiation is governed by the stellar insolation. Very sophisticated atmosphere models of exoplanets are being developed (Seager et al. 2000; Hubeny et al. 2003; Barman et al. 2005; Burrows et al. 2008; Fortney et al. 2008). At the same time, models with various simplifications are often very useful to study various effects (Hansen 2008; Kipping & Tinetti 2009; Madhusudhan & Seager 2009; Cowan & Agol 2010).

##### 4.1. Shapes of the transiting extrasolar planets

Our knowledge about the size of exoplanets comes mainly from the observations of transits. A majority of exoplanet studies assume that the exoplanets have a spherical shape. The precision of the photometric measurements is advancing revealing more and more details. Recently, Kipping & Tinetti (2009) attempted to model the light curve and transit assuming the spherical shape but taking into account the intrinsic night side emission of the planet during the transit. They found that in the infrared region the effect is of the order of  $10^{-4}$ . Seager & Hui (2002), Barnes & Fortney (2003), Carter & Winn (2010) assumed the shape of the rotational ellipsoid. Welsh et al. (2010) used the Roche potential approximation to describe the shape of the parent star and to explain the ellipsoidal variations of HAT-P-7. Nevertheless, many transiting exoplanets are so close to their host stars that their shape is best described by the Roche model. Very recently, Li et al. (2010) developed a very sophisticated model for the tidally distorted exoplanet WASP-12b.

Our code was applied to transiting extrasolar planets and exact Roche model shape of all the transiting exoplanets was calculated. Circular orbit with the radius equal to the semi-major axis and synchronized rotation of the planet was assumed. The results are displayed in the Table 1. It lists  $R_{sub}$ ,  $R_{back}$ ,  $R_{pole}$ ,  $R_{side}$ ,  $R_{eff}$  which are the radii at the sub-stellar point, anti-stellar point, rotation pole, on the side, and the effective radius of the planet, i.e. the radius of the sphere with the same volume as the Roche surface, respectively. Departures from the sphere are measured by the value of the  $R_{sub}/R_{pole}$ . It was also assumed that the observed radius of the planet is equal to  $R_{side}$  which has almost no effect on the relative proportions of most of the planets but may slightly underestimate the departures from the sphere for a few highly distorted planets.

One can see that the departures from the spherical shape vary by several orders of magnitude. Departures of about 1% are common. About 8% of planets (all of them have semi-major axis smaller than 0.03 AU) have departures larger than 3%. These include: OGLE-TR-56b, WASP-4b, and CoRoT-1b. The extreme cases are WASP-12b, WASP-19b, and WASP-33b when the departures can exceed 14%, 12% and 8%, respectively. This is clearly comparable to the precision of the planet radius determination or the transit radius effect. Moreover, this shape distortion would be even higher if one was to consider the eccentricity of the orbit and assume the periastron distance instead of the semi-major axis. The highest departures seem to be along the line joining the objects (the  $R_{sub}/R_{pole}$  parameter) which would affect mainly the overall light-curve. During the transit event, it is mainly  $R_{side}/R_{pole}$  parameter which is most relevant and this does not acquire such high values (about 2% in case of WASP-12b, WASP-19b, and WASP-33b).

The observed radius of the planet should be associated with the cross-section of the planet during the transit which is represented by  $R_{side}, R_{pole}$ . On the other hand, theoretical radius, e.g. from the evolutionary calculations, might be associated rather with the effective radius of the planet. One has to keep the findings above in mind when interpreting the planet radius measurements or calculations (Guillot & Showman 2002; Burrows et al. 2007; Fortney et al. 2007; Baraffe et al. 2008;

Lecointe et al. 2010).

Apart from the shape of these planets, I calculated also a temperature distribution over the surface for all these exoplanets. This is rather cumbersome to tabulate and the result depends heavily on the free parameters of the model that is why I provide the reader with the code which can do that. In the Table 1 only the mean temperature of each transiting planet is listed. This was calculated assuming its Roche shape and  $A_B = 0.1, P_r = 0.5, P_a = 0.5, T_{old} = 100K$ . These mean temperatures vary considerably from 300 to 2600K. The hottest planets are WASP-33b, WASP-12b, and WASP-18b with the mean temperatures of about 2600, 2430, and 2330 K, respectively. The separation of these extremely hot planets from the host star is smaller than 0.03 AU and temperatures of planets at a wider separation decrease accordingly.

#### 4.2. Light curves of the extrasolar planets

In this section, we apply our model to the light-curves of extrasolar planets HD189733b and Wasp-12b. We will start with HD189733b. The planet properties were determined by Winn et al. (2007). Knutson et al. (2007) obtained superb light curve of the planet which covers more than half of the orbit. It was observed at 8 micron in the infrared region.

First, let us introduce the qualitative distribution of the temperature over the surface of HD189733b produced by our model. Fig.1 illustrates the behaviour of the temperature for a relatively intense heat redistribution factor  $P_r = 0.6$  and quite small zonal temperature redistribution parameter  $P_a = 0.1$  (i.e. intense flows along parallels but not very intense heat flows along meridians). One can observe that this model produces hotter regions at the sub-stellar point and near the equator while cooler regions are at the poles. Fig.2 then illustrates the behaviour of the intensity. This is what would an observer see looking on the planet pole-on. Limb darkening was applied to the model. One would see the dark polar regions, however, the hot sub-stellar point would not be the brightest since all hotter equatorial regions would be dim due to the limb darkening. Black body approximation was used to model the energy distribution.

Now, we can proceed to a comparison between the observations of Knutson et al. (2007) and models produced by SHELLSPEC shown in Fig.3. The synthetic light-curves are very sensitive to the heat redistribution parameter  $P_r = \langle 0, 1 \rangle$ . Especially, at the phases close to the transit, when the night side of the planet is seen, the flux can change by the orders of magnitude. The best fit is obtained for  $P_r = 0.5 - 0.8$ , which means that the surface heat redistribution is crucial and quite effective. This finding is in agreement with the results of Knutson et al. (2007), Burrows et al. (2008), Madhusudhan & Seager (2009), and Cowan & Agol (2010).

Albedo is an important parameter at all wavelengths. The effect of the wavelength independent Bond albedo is illustrated in Fig.4. Our models indicate that Bond albedo of this planet is relatively small of about 0.1 which is in agreement with Cowan & Agol (2010). Higher albedo reflects more light which could be observed especially at the shorter wavelengths. This reflected light might be relatively small in the IR region. However, higher albedo reduces the amount of energy absorbed and redistributed over the surface. Surface temperatures are lower which manifests in lower fluxes at longer wavelengths.

It is interesting to see that these kinds of light curves of transiting exoplanets are not very sensitive to the zonal temperature redistribution parameter  $P_a = \langle 0, 1 \rangle$  associated with the effectiveness of the homogeneous heat transfer versus zonal transfer. It is illustrated in Fig.4 too. If the heat flows mainly along the equator and not along the meridians ( $P_a = 0$ ) and we view the planet almost edge-on then we observe a slight increase of flux at all phases, especially on the night side (compared to the homogeneous temperature distribution,  $P_a = 1$ ).

It is also interesting to observe a moderate effect of the limb darkening on such light-curves of transiting exoplanets. Limb darkening is manifested mainly shortly before and after the transit and near the secondary eclipse. See Fig.5 with the comments and the description. It might be interesting to point out that extrasolar planets might show limb brightening at some wavelengths. This depends on the temperature gradient at a particular depth probed by a certain wavelength. If the temperature is decreasing one would observe the

limb darkening. If it is increasing one would observe limb brightening. There are two main effects which could cause the temperature inversion. (1) Presence of species high in the atmosphere effectively absorbing near the wavelength of maximum of the stellar energy redistribution. This would cause the temperature inversion often called a stratosphere. (2) Heat redistribution between the day and the night side, especially if it occurs at deeper layers (Burrows et al. 2008). This might significantly cool such layers on the day side producing a drop in the temperature and associated temperature inversion. This is the main motivation why we study also the effect of limb brightening on the Fig.5 and its effect is just the opposite of the limb darkening. It might be worth mentioning that all the above mentioned calculations took into account the proper inclination of the orbit. Depending how close to edge-on the planet's orbit is, the observed light curve may vary by 5% simply due to the observer's viewing angle (Cowan & Agol 2008).

However, there are cases when the zonal temperature redistribution parameter,  $P_a$ , and limb darkening will be much more important. Fig.6 illustrates the situation for a hypothetical planet at an inclination of 20 degrees. We used the parameters for the non-transiting extrasolar planet HD179949b (Tinney et al. 2001; Cowan et al. 2007) to feed the code with real numbers. However, inclination, mass and radius are not known for non-transiting exoplanets. In this case the effects of the zonal temperature redistribution parameter and limb darkening are indeed important and are comparable to the amplitude of the light curve. Another point worth making is that there will be a strong degeneracy between the radius,  $P_r$ , and inclination since all of them affect the amplitude of the light-curve. Also there may be a degeneracy between  $P_a$ , limb darkening and radius since all of them affect the mean level of the light-curve. This justifies the complexity of our model with the heat redistribution and zonal temperature redistribution, and limb darkening parameters. Gravity darkening is also included but this will not be an issue for the extrasolar planets. If they are close to the star then their intrinsic radiation is negligible compared to the heavy external irradiation and if they are far from the star then their shape will be almost spherical

(neglecting the rotation) and without the gravity darkening.

Finally, let us study how this Roche shape might affect the light-curve of an extrasolar planet. This is illustrated Fig.7 on the example of WASP-12b at 8 micron. The light varies by about 10% as predicted by Li et al. (2010). However, the most striking thing is the double humped light-curve in case of effective heat redistribution  $P_r = 1$ . This shape of the light-curve gradually changes to a typical single humped shape for less intense heat redistribution (lower values of  $P_r$ ). The transition to a single humped light-curve is color dependent and for shorter wavelengths occurs at higher  $P_r$ . These calculations assumed the proper inclination of the orbit, zero albedo, zero limb darkening, and  $P_a = 1$ . Assuming  $A_B = 0, P_r = 1, P_a = 1, T_{old} = 100K$  and Roche shape we got the mean temperature of the planet of 2470 K which is in good agreement with 2516K obtained by Hebb et al. (2009) who assumed the spherical shape.

In the next step we calculated the light-curves of the planet at much shorter wavelength (0.9 micron) and attempted to understand the secondary eclipse observations of Lopez-Morales et al. (2009). This is illustrated in Fig.8. Notice that at this shorter wavelength the light-curves cover a considerable range of values during the secondary eclipse. This is contrary to the longer wavelengths when light-curves have higher spread during the transit. There is a lot of degeneracy between the albedo and heat redistribution in this case. For example the observation of Lopez-Morales et al. (2009) can be reproduced equally well by the model with  $A_B = 0, P_r = 0.25$  with the mean surface temperature 2470 K as well as by the model with  $A_B = 0.95, P_r = 1$  with the mean surface temperature of 1170K. Note that heat redistribution is not very important nor well constrained if the albedo is very high. It is also possible to fit the observations assuming that the surface is not reflective and the temperature is homogeneous over the entire surface ( $A_B = 0, P_r = 1, P_a = 1$ ) and adopting  $T_{old} = 2600K$ . This corresponds to the mean temperature of the planet of about 3000K (in this case the mean temperature is identical to the effective temperature and to the brightness temperature of the body). This is much higher than a day side brightness temperature of 2660 K reported by Lopez-Morales et al. (2009) but it

is in perfect agreement with the value of 2997 K given by Cowan & Agol (2010).

### 4.3. Spectra of the extrasolar planets

I would like to point out that this paper does not deal with the calculations of the local atmosphere models and intensity emerging from the local atmosphere models on the surface of the planet or star. However, in case grids of such models and spectra are available (Hubeny & Burrows 2007; Allard et al. 2003) they can be used as an input to our model and composite spectra of the star and/or planet can be calculated from optional view point. In this respect, our code is not restricted to the black body approximation.

In this section we apply our model to WASP-19b and study its spectrum. This planet was discovered by Hebb et al. (2010). The secondary eclipse was detected in the H-band by Anderson et al. (2010b). The authors found the emission from the planet very strong and it presents an interesting puzzle for the models. This is a highly distorted exoplanet and we assumed a proper shape according to the Roche potential, proper inclination, zero heat redistribution, homogeneous zonal temperature redistribution, zero limb and gravity darkening and calculated spectra during the secondary eclipse. It was also assumed that the star has a spectrum given by Castelli & Kurucz (2004). As a first approximation for the planet I used the black body approximation. The comparison of the data with our model is in Fig.9. Our black body model with zero albedo and zero heat redistribution  $P_r = 0$  still under-predicts the radiation from the planet but it is within  $2\sigma$  from the measurements.

This figure also illustrates the effect of the albedo on the spectrum. For example, relatively small frequency independent (grey) albedo of about 0.2 will strongly increase the planet radiation at the shorter wavelengths but decrease the fluxes from the planet at wavelengths longer than 0.9 micron. This is because the non-zero albedo reduces the surface temperature of the planet but reflects the stellar light at shorter wavelengths. In the next step we assumed that the albedo is not grey but has the following color dependence

$$A_\nu = \frac{A_0(\lambda/\lambda_0)^\gamma}{(1 - A_0) + A_0(\lambda/\lambda_0)^\gamma}. \quad (34)$$

where  $A_0$  is albedo at some reference wavelength  $\lambda_0$ . We set  $\gamma = -4$  to mimic the Rayleigh scattering with  $\lambda^{-4}$  dependence and adjust  $A_0$  to recover the same Bond albedo (0.2) as in the previous case. This case produces identical surface temperatures as in the grey albedo case but radiation below 0.6 micron is considerably higher than in the grey case, radiation above the 0.6 micron is lower than in the grey case, and at still longer wavelength the relative difference between the grey and color albedo calculations gradually decreases. Finally, I refrained from the black-body approximation for the planet and used the grid of non-irradiated atmosphere models of Hubeny & Burrows (2007) for  $T_{eff} < 1800K$  and Allard et al. (2003) (BT-Settl) for  $T_{eff} > 1800K$ . With this approach one can fit the observations of Anderson et al. (2010b) reasonably well. The fit requires that the planet has low Bond albedo and low heat redistribution. The stratosphere, if present, should not have drastic impact on the spectrum since if the JHK band were reversed and were in absorption (instead of emission) it might be difficult to conserve the total flux and fit these observations simultaneously.

## 5. Conclusions - Summary

I argue that the reflection effect in the interacting binaries must be revisited in order to describe properly the radiation from the cool object irradiated by the hot object. Subsequently, a new model for the reflection effect was proposed and applied to an extreme case of an interacting binary - extrasolar planet.

The new model introduces several free parameters. Some of them are well known in the field of extrasolar planets. (1) Bond albedo  $A_B = < 0, 1 >$  which controls how much energy is reflected and how much is converted into the heat.  $A_B = 1$  means that all impinging energy is reflected off the surface and nothing gets converted into the heat. (2) Heat redistribution parameter  $P_r = < 0, 1 >$  which controls how much heat from a certain point is redistributed to other places and how much is re-radiated locally.  $P_r = 0$  means that all absorbed heat is re-radiated locally and nothing gets transported to other places. (3) Zonal temperature redistribution parameter  $P_a = < 0, 1 >$  is a measure of the effectiveness of the homogeneous heat

redistribution over the surface versus the zonal distribution.  $P_a = 1$  means that the heat is homogeneously redistributed over the surface while  $P_a = 0$  means zonal redistribution and that the heat flows only along the parallels. Our model properly describes the shapes of the objects by means of the Roche potential and takes into account gravity and limb darkening. At the same time it takes into account the orbital revolution, rotation and proper Doppler shifts in the scattered and thermal radiation.

It is demonstrated on HD189733b that the light-curves of transiting extrasolar planets are mainly sensitive to the heat redistribution parameter  $P_r$  and not so sensitive to the zonal temperature redistribution parameter  $P_a$  or to the limb darkening. However, light-curves of planets seen at very low inclinations are very sensitive also to the zonal temperature redistribution parameter  $P_a$  as well as to the limb darkening. This planet has low Bond albedo and relatively intense heat redistribution.

The effect of non-spherical shape on the light-curve can also be important. For highly distorted planets like WASP-12b this might cause a double humped curve with the amplitude of about 10% superposed on other types of variability. Observations of this planet at 0.9 micron cannot constrain the Bond albedo or heat redistribution well.

The effect of the grey and non-grey albedo on the spectrum of the Wasp-19b was studied as well. It was demonstrated that non-blackbody model with fluxes given by non-irradiated atmosphere models (Hubeny & Burrows 2007; Allard et al. 2003) can fit the observations of Anderson et al. (2010b) reasonably well. The planet has low Bond albedo and low heat redistribution.

We calculated the exact Roche shapes of all currently known transiting exoplanets (Schneider 1995) and found out that the departures from spherical symmetry may vary significantly. Departures of the order of 1% are common, and can exceed about 8% in most extreme cases like WASP-12b, WASP-19b, and WASP-33b. About 8% of transiting planets have departures more than 3% (all have semi-major axes smaller than 0.03 AU). Temperature redistribution over the surface of all these planets was also calculated. The mean temperatures of the planets also vary considerably from 300 K to 2600 K. The extreme cases

are WASP-33b, WASP-12b, and WASP-18b with mean temperatures of about 2600, 2430, and 2330 K, respectively.

I thank Nick Cowan for valuable comments on the manuscript and Heather Knutson for sharing a copy of her data. The author acknowledges the support from the Marie Curie International Reintegration grant FP7-200297 and partial support from the VEGA grants 2/0078/10, 2/0074/09.

## REFERENCES

- Allard, F., Guillot, T., Ludwig, H.-G., Hauschildt, P.H., Schweitzer, A., Alexander, D.R., & Ferguson, J.W. 2003, Proceedings of IAU Symposium No.211, 325
- Alonso, R. et al. 2004, ApJ, 613, L153
- Alonso, R. et al. 2008, A&A, 482, L21
- Anderson, D.R. et al. 2010, ApJ, 709, 159
- Anderson, D.R. et al. 2010, A&A, 513, L3
- Bakos, G. et al. 2007a, ApJ, 671, L173
- Bakos, G. et al. 2007b, ApJ, 656, 552
- Bakos, G. et al. 2009a, ApJ, 707, 446
- Bakos, G. et al. 2009b, ApJ, 696, 1950
- Bakos, G. et al. 2010, ApJ, 710, 1724
- Baraffe, I., Chabrier, G., & Barman, T. 2008, A&A, 482, 315
- Barge, P. et al. 2008, A&A, 482, L17
- Barman, T.S., Hauschildt, P.H., & Allard, F. 2005, ApJ, 632, 1132
- Barnes, J.W., & Fortney, J.J. 2003, ApJ, 588, 545
- Bean, J.L. et al. 2008, A&A, 486, 1039
- Borucki, W.J. et al. 2010, ApJ, 713, L126
- Borucki, W.J. et al. 2010b, Science 327, 977
- Bouchy, F. et al. 2005, A&A, 444, L15
- Bouchy, F. et al. 2010, A&A, accepted
- Bradstreet, D.H., & Steelman, D.P. 2002, BAAS, 34, 1224

- Budaj, J., Burrows, A., Hubeny, I., & Ibgui, L. 2009, poster at GA in Rio de Janeiro
- Budaj, J., & Richards, M.T. 2004, *Contrib. Astron. Obs. Skalnaté Pleso*, 34, 167
- Budaj, J., Richards, M.T., & Miller, B. 2005, 2005, *ApJ*, 623, 411
- Burke, C. et al. 2007, *ApJ*, 671, 2115
- Burke, C. et al. 2008, *ApJ*, 686, 1331
- Burrows, A., Budaj, J., & Hubeny, I. 2008, *ApJ*, 678, 1436
- Burrows, A., Hubeny, I., Budaj, J., & Hubbard, W. B. 2007, *ApJ*, 661, 502
- Burrows, A., Sudarsky, D., & Hubeny I. 2006, *ApJ*, 650, 1140
- Castelli, F., Kurucz, R.L. 2004, arXiv:0405087
- Carter, J.A., & Winn, J.N. 2010, *ApJ*, 709, 1219
- Charbonneau, D. et al., 2009, *Nature*, 462, 891
- Collier Cameron, A. et al. 2007, *MNRAS*, 380, 1230
- Collier Cameron, A. et al. 2010, *MNRAS*, submitted
- Cowan, N.B., Agol, E. 2008, *ApJ*, 678, L129
- Cowan, N.B., & Agol, E. 2010, arXiv:1001.0012
- Cowan, N.B., Agol, E., & Charbonneau, D. 2007, *MNRAS*, 379, 641
- Daemgen, S., Hormuth, F., Brandner, W., Bergfors, C., Janson, M., Hippler, S., & Henning, T. 2009, *A&A*, 498, 567
- Deeg, H.J. et al. 2010, *Nature*, 464, 384
- Deleuil, M. et al. 2008, *A&A*, 491, 889
- Djurasevic, G. 1992, *Ap&SS*, 197, 17
- Dobbs-Dixon, I., & Lin, D. N. C. 2008, *ApJ*, 673, 513
- Drechsel, H., Haas, S., Lorenz, R., & Mayer, P. 1994, *A&A*, 284, 853
- Dunham, E.W. et al. 2010, *ApJ*, 713, L136
- Enoch, B. et al. 2010, *MNRAS*, submitted
- Fortney, J.J., Lodders, K., Marley, M.S., & Freedman, R.S. 2008, *ApJ*, 678, 1419
- Fortney, J.J., Marley, M.S., & Barnes, J.W. 2007, *ApJ*, 659, 1661
- Fossey, S.J., Waldmann, I.P., & Kipping, D.M. 2009, *MNRAS*, 396, L16
- Fridlund, M. et al. 2010, *A&A*, 512, A14
- Gibson, N.P. et al. 2008, *A&A*, 492, 603
- Gillon, M., Pont, F., Moutou, C., Bouchy, F., Courbin, F., Sohy, S., & Magain, P. 2006, *A&A*, 459, 249
- Gillon, M. et al. 2007, *A&A*, 466, 743
- Gillon, M. et al. 2009, *A&A*, 501, 785
- Guillot, T., Burrows, A., Hubbard, W.B., Lunine, J.I., & Saumon, D. 1996, *ApJ*, 459, L35
- Guillot, T., & Showman, A. P. 2002, *A&A*, 385, 156
- Hadrava, P. 1997, *A&AS*, 122, 581
- Hansen, B.M.S. 2008, *ApJS*, 179, 484
- Hartman, J.D. et al. 2009, *ApJ*, 706, 785
- Hebb, L. et al. 2009, *ApJ*, 693, 1920
- Hebb, L. et al. 2010, *ApJ*, 708, 224
- Hellier, C. et al. 2009, *ApJ*, 690, L89
- Hellier, C. et al. 2010, preprint
- Henry, G.W., Marcy, G.W., Butler, R.P., & Vogt, S.S. 2000, *ApJ*, 529, L41
- Hill, G. 1979, *Publ. Dom. Ap. Obs. Victoria* 15, 297
- Hubeny, I., Burrows, A., & Sudarsky, D. 2003, *ApJ*, 594, 1011
- Hubeny, I., & Burrows, A. 2007, *ApJ*, 669, 1248
- Jenkins, J.M. et al. 2010, arXiv:1001.0416
- Johnson, J.A., Winn, J.N., Cabrera, N.E., & Carter, J.A. 2009, *ApJ*, 692, L100

- Johns-Krull, C. et al. 2008, *ApJ*, 677, 657
- Joshi, Y.C. et al. 2008, *MNRAS*, 392, 1532
- Kallrath, J., Milone, E.F., Terrell, D., & Young, A.T. 1998, *ApJ*, 508, 308
- Kipping, D.M., & Tinetti, G. 2009, arXiv:0912.1133
- Knutson, H. et al. 2007, *Nature*, 447, 183
- Kopal, Z. 1959, *Close Binary Systems*, London, Chapman & Hall Ltd.
- Kovacs, G. et al. 2007, *ApJ*, 670, L41
- Latham, D.W. et al. 2009, *ApJ*, 704, 1107
- Latham, D.W. et al. 2010, *ApJ*, 713, L140
- Lecante, J., Chabrier, G., Baraffe, I., & Levrard, B. 2010, arXiv:1004.0463
- L'eger A. et al. 2009, *A&A*, 506, 287
- Li, S-L, Miller, N., Lin, D.N.C., & Fortney, J.J. 2010, *Nature*, 463, 1054
- Linnell, A.P., & Hubeny, I. 1996, *ApJ*, 471, 958
- Lister, T.A. et al. 2009, *ApJ*, 703, 752
- Lucy, L.B. 1968, *ApJ*, 153, 877
- Madhusudhan, N., & Seager, S. 2009, *ApJ*, 707, 24
- Maxted, P.F.L. et al. 2010, arXiv:1004.1514
- McCullough, P.R. et al. 2006, *ApJ*, 648, 1228
- McCullough, P.R. et al. 2008, arXiv:0805.2921
- Menou, K., & Rauscher, E. 2009, *ApJ*, 700, 887
- Mochnacki, S.W., & Doughty, N.A. 1972, *MNRAS* 156, 51
- Lopez-Morales, M., Coughlin, J., Sing, D., Burrows, A., Apai, D., Rogers, J.C., Spiegel, D.S. 2009, arXiv:0912.2359
- Moutou, C. et al. 2008, *A&A*, 488, L47
- Noyes, R.W. et al. 2008, *ApJ*, 673, L79
- O'Donovan, F.T. et al. 2007, *ApJ*, 663, L37
- Orosz, J.A. & Hauschildt, P.H. 2000, *A&A*, 364, 265
- Pál, A. et al. 2009, *MNRAS*, 401, 2665
- Pavlovski, K., Burki, G., & Mimica, P. 2006, *A&A*, 454, 855
- Plavec, M., & Kratochvil, P. 1964, *Bull. Astron. Inst. Czechoslovakia*, 15, 165
- Pont, F., Bouchy, F., Queloz, D., Santos, N.C., Melo, C., Mayor, M., & Udry S. 2004, *A&A*, 426, L15
- Pont, F. et al. 2007, *A&A*, 465, 1069
- Pont, F. et al. 2008, *A&A*, 487, 749
- Popper, D.M., & Etzel, P.B. 1981, *AJ*, 86, 102
- Pribulla, T. 2004, in *Spectroscopically and Spatially Resolving the Components of Close Binary Stars*, R.W. Hilditch et al. (eds.), ASP Conf. Series., 318, 117
- Prša, A., & Zwitter, T. 2005, *ApJ*, 628, 426
- Rauer, H. et al. *A&A*, 506, 281
- Rucinski, S.M. 1969, *Acta Astronomica*, 19, 245
- Rucinski, S.M. 1973, *Acta Astronomica*, 23, 79
- Sahu, K.C. et al. 2006, *Nature*, 443, 534
- Sato, B. et al. 2005, *ApJ*, 633, 465
- Schneider, J., 1995, *The Extrasolar Planets Encyclopaedia*, <http://exoplanet.eu>
- Seager, S., Whitney, B.A., Sasselov, D.D. 2000, *ApJ*, 540, 504
- Seager, S., & Hui, L. 2002, *ApJ*, 574, 1004
- Showman, A.P., Fortney, J.J., Lian, Y., Marley, M.S., Freedman, R.S., Knutson, H.A., & Charbonneau, D. 2009, *ApJ*, 699, 564
- Shporer, A. et al. 2009, *ApJ*, 690, 1393
- Skillen, I. et al. 2009, *A&A*, 502, 391
- Smalley, B. et al. 2010, *A&A*, submitted
- Smith, A.M.S. et al. 2009, *MNRAS*, 398, 1827
- Southworth, J. et al. 2009a, *ApJ*, 707, 167

Southworth, J. et al. 2009b, MNRAS, 399, 287

Southworth, J. et al. 2009c, MNRAS, 396, 1023

Street, R. et al. 2010, ApJ, submitted

Sudarsky, D., Burrows, A., Hubeny, I., & Li, A. 2005, ApJ, 627, 520

Tamuz, O., Mazeh, T., & North, P. 2006, MNRAS, 367, 1521

Tkachenko, A., Lehmann, H., & Mkrtichian, D. 2010, AJ, 139, 1327

Tinney, C. G., Butler, R.P., Marcy, G.W., Jones, H.R.A., Penny, A.J., Vogt, S.S., Apps, K., & Henry, G.W. 2001, ApJ, 551, 507

Torres, G. et al. 2007, ApJ, 666, L121

Torres, G. et al. 2010, ApJ, 715, 458

Udalski. A. et al. 2008, A&A, 482, 299

Weldrake, D.T.F., Bayliss, D.D.R., Sackett, P.D., Tingley, B.W., Gillon, M., & Setiawan, J. 2008, ApJ, 675, L37

Welsh, W.F., Orosz, J.A., Seager, S., Fortney, J.J., Jenkins, J., Rowe, J.F., Koch, D., & Borucki, W.J. 2010, ApJ, 713, L145

West, R.G. et al. 2009, AJ, 137, 4834

West, R. et al. 2010, ApJ, submitted

Wilson, R.E., & Devinney, E.J. 1971, ApJ 166, 605

Wilson, R.E. 1990, ApJ, 356, 613

Winn, J.N. et al. 2007, AJ, 133, 1828

Winn, J.N. et al. 2009, ApJ, 693, 794

Wood, D.B. 1971, AJ, 76, 701

Zhang, E.-H., Robinson, E.L., & Nather, R.E. 1986, ApJ, 305, 740

Table 1: Shapes of the transiting exoplanets. Columns are:  $a$  -semi-major axis in [AU],  $q$  -star/planet mass ratio,  $R_{sub}$  -planet radius at the sub-stellar point ( $R_{sub},0,0$ ),  $R_{back}$  -planet radius at the anti-stellar point,  $R_{pole}$  -planet radius at the rotation pole ( $0,0,R_{pole}$ ),  $R_{side}$  -planet radius at the side point ( $0,R_{side},0$ ), (assumed equal to the planet radius determined from the transit),  $R_{eff}$  -effective radius of the planet,  $rr = R_{sub}/R_{pole}$  -departure from the sphere,  $f_i = R_{sub}/L_{1x}$  -fill-in parameter of the Roche lobe,  $T$  -mean temperature of the planet in K. Radii are in units of Jupiter radius. Coordinates of the center of mass of the planet are  $(0,0,0)$ . See the text for a more detailed information.

name	a	q	Rsub	Rback	Rpole	Rside	Reff	rr	$f_i$	T	Reference
GJ 1214b	0.01400	9186	0.24342	0.24340	0.24088	0.24150	0.24192	1.01053	0.253	551	Charbonneau et al. (2009)
WASP-19b	0.01640	865	1.43896	1.42960	1.28052	1.31000	1.33680	1.12373	0.590	1914	Hebb et al. (2010)
CoRoT-7b	0.01720	64503	0.15108	0.15107	0.14965	0.15000	0.15024	1.00952	0.244	1760	L'eger et al. (2009)
WASP-18b	0.02047	128	1.16966	1.16949	1.16349	1.16500	1.16601	1.00531	0.208	2329	Southworth et al. (2009a)
OGLE-TR-56b	0.02250	949	1.34392	1.34211	1.28736	1.30000	1.30950	1.04393	0.414	1967	Pont et al. (2007)
TrES-3	0.02260	504	1.31652	1.31569	1.28839	1.29500	1.29967	1.02183	0.329	1606	O'Donovan et al. (2007)
WASP-12b	0.02290	1002	1.98765	1.97291	1.74650	1.79000	1.83079	1.13808	0.613	2407	Hebb et al. (2009)
OGLE-TR-113b	0.02290	618	1.10252	1.10213	1.08607	1.09000	1.09273	1.01515	0.290	1114	Gillon et al. (2006)
WASP-4b	0.02300	840	1.46767	1.46538	1.40130	1.41600	1.42715	1.04736	0.425	1815	Southworth et al. (2009b)
CoRoT-1b	0.02540	966	1.54395	1.54167	1.47462	1.49000	1.50166	1.04702	0.424	1835	Barge et al. (2008)
WASP-33b	0.02560	1410	1.66033	1.65542	1.53414	1.56000	1.58143	1.08225	0.512	2582	Cameron et al. (2010)
WASP-5b	0.02729	653	1.18130	1.18101	1.16773	1.17100	1.17325	1.01162	0.266	1737	Southworth et al. (2009c)
CoRoT-2b	0.02810	306	1.47584	1.47548	1.46154	1.46500	1.46736	1.00979	0.253	1495	Alonso et al. (2008)
GJ 436b	0.02822	6574	0.43970	0.43968	0.43744	0.43800	0.43838	1.00516	0.200	695	Bean et al. (2008)
SWEEPS-11	0.03000	118	1.13119	1.13116	1.12961	1.13000	1.13026	1.00140	0.134	1959	Sahu et al. (2006)
OGLE-TR-132b	0.03060	1157	1.19343	1.19309	1.17577	1.18000	1.18294	1.01503	0.288	1925	Gillon et al. (2007)
HD 189733b	0.03099	741	1.14505	1.14488	1.13573	1.13800	1.13955	1.00821	0.236	1178	Bouchy et al. (2005)
WASP-2b	0.03138	962	1.02260	1.02249	1.01519	1.01700	1.01823	1.00730	0.227	1258	Daemgen et al. (2009)
WASP-3b	0.03170	737	1.32162	1.32131	1.30630	1.31000	1.31254	1.01172	0.266	1930	Gibson et al. (2008)
TrES-2	0.03556	856	1.28042	1.28022	1.26929	1.27200	1.27385	1.00876	0.241	1455	Daemgen et al. (2009)
WASP-24b	0.03590	1145	1.11018	1.11006	1.10200	1.10400	1.10536	1.00742	0.228	1611	Street et al. (2010)
XO-2b	0.03690	1800	0.97839	0.97830	0.97126	0.97300	0.97419	1.00735	0.226	1281	Burke et al. (2007)
WASP-14b	0.03700	178	1.26047	1.26044	1.25851	1.25900	1.25932	1.00156	0.138	1802	Joshi et al. (2008)
WASP-10b	0.03710	243	1.08107	1.08105	1.07965	1.08000	1.08024	1.00132	0.130	1008	Johnson et al. (2009)
HAT-P-7b	0.03790	855	1.43186	1.43160	1.41753	1.42100	1.42338	1.01011	0.253	2075	Welsh et al. (2010)
WASP-1b	0.03820	1459	1.37324	1.37289	1.35319	1.35800	1.36134	1.01482	0.287	1749	Cameron et al. (2007)
HAT-P-12b	0.03840	3623	0.96819	0.96804	0.95607	0.95900	0.96102	1.01267	0.271	930	Hartman et al. (2009)
HAT-P-3b	0.03894	1636	0.89290	0.89285	0.88905	0.89000	0.89064	1.00432	0.190	1119	Torres et al. (2007)
TrES-1	0.03930	1493	1.08664	1.08654	1.07917	1.08100	1.08224	1.00692	0.222	1050	Alonso et al. (2004)
WASP-26b	0.04000	1150	1.32922	1.32902	1.31704	1.32000	1.32202	1.00924	0.245	1615	Smalley et al. (2010)
HAT-P-5b	0.04075	1146	1.26718	1.26704	1.25768	1.26000	1.26158	1.00755	0.229	1496	Bakos et al. (2007a)
OGLE-TR-10b	0.04162	1961	1.27165	1.27142	1.25209	1.26000	1.26256	1.01223	0.268	1238	Pont et al. (2007)
WASP-6b	0.04210	2456	1.23659	1.23635	1.22000	1.22400	1.22677	1.01360	0.278	1353	Gillon et al. (2009)
WASP-16b	0.04210	1251	1.01088	1.01084	1.00706	1.00800	1.00864	1.00380	0.182	1235	Lister et al. (2009)
HAT-P-13b	0.04260	1503	1.28881	1.28863	1.27717	1.28000	1.28194	1.00911	0.243	1600	Bakos et al. (2009a)
HD 149026b	0.04313	3792	0.65543	0.65542	0.65353	0.65400	0.65432	1.00291	0.165	1700	Sato et al. (2005)
HAT-P-10b	0.04390	1867	1.04940	1.04933	1.04357	1.04500	1.04597	1.00558	0.206	1004	Bakos et al. (2009b)
HAT-P-4b	0.04460	1940	1.27961	1.27944	1.26692	1.27000	1.27211	1.01042	0.251	1641	Kovacs et al. (2007)
XO-3b	0.04540	107	1.21742	1.21741	1.21686	1.21700	1.21709	1.00046	0.092	1662	West-Krull et al. (2008)
WASP-28b	0.04550	1243	1.12346	1.12340	1.11887	1.12000	1.12076	1.00410	0.187	1375	Johnson et al. (2010)
Kepler-4b	0.04560	16634	0.35747	0.35747	0.35684	0.35700	0.35710	1.00175	0.139	1570	Borucki et al. (2010)
WASP-29b	0.04560	3479	0.74183	0.74181	0.73940	0.74000	0.74040	1.00338	0.172	970	Hellier et al. (2010)
Kepler-6b	0.04567	1892	1.33329	1.33310	1.31970	1.32300	1.32526	1.01030	0.253	1461	Dunham et al. (2010)
Lupus-TR-3b	0.04640	1124	0.89117	0.89115	0.88951	0.89000	0.89026	1.00175	0.140	987	Weldrake et al. (2008)
WASP-22b	0.04680	2057	1.15238	1.15230	1.14828	1.15000	1.15116	1.00246	0.214	1384	Maxted et al. (2010)
OGLE-TR-111b	0.04700	1620	1.07037	1.07032	1.06590	1.06700	1.06774	1.00419	0.188	987	Pont et al. (2004)
HD 209458b	0.04707	1544	1.32755	1.32742	1.31756	1.32000	1.32166	1.00759	0.229	1375	Henry et al. (2000)
WASP-25b	0.04740	1805	1.26718	1.26705	1.25768	1.26000	1.26158	1.00755	0.228	1207	Enoch et al. (2010)
Kepler-8b	0.04830	2106	1.43187	1.43162	1.41490	1.41900	1.42183	1.01200	0.266	1616	Jenkins et al. (2010)
XO-5b	0.04870	855	1.09073	1.09070	1.08843	1.08900	1.08938	1.00211	0.150	1207	Burke et al. (2008)
HAT-P-8b	0.04870	882	1.50647	1.50635	1.49790	1.50000	1.50142	1.00573	0.209	1658	Latham et al. (2009)
XO-1b	0.04880	1163	1.18727	1.18722	1.18293	1.18400	1.18472	1.00367	0.180	1208	McCullough et al. (2006)
CoRoT-5b	0.04947	2242	1.39965	1.39943	1.38428	1.38800	1.39056	1.01110	0.259	1400	Rauer et al. (2009)
WASP-15b	0.04990	2280	1.44095	1.44071	1.42387	1.42800	1.43085	1.01200	0.266	1607	West et al. (2009)
Kepler-5b	0.05064	680	1.43466	1.43459	1.42980	1.43100	1.43180	1.00340	0.176	1758	Borucki et al. (2010b)
TrES-4	0.05091	1577	1.82048	1.81998	1.79224	1.79900	1.80371	1.01576	0.292	1705	Daemgen et al. (2009)
OGLE-TR-211b	0.05100	1352	1.36583	1.36573	1.35810	1.36000	1.36128	1.00569	0.208	1683	Udalski et al. (2008)
OGLE-TR-182b	0.05100	1182	1.13241	1.13238	1.12921	1.13000	1.13053	1.00284	0.165	1315	Pont et al. (2008)
WASP-17b	0.05100	2564	1.77093	1.77022	1.73048	1.74000	1.74678	1.02337	0.333	1594	Anderson et al. (2010)
WASP-21b	0.05200	3526	1.07550	1.07543	1.06821	1.07000	1.07121	1.00682	0.220	1229	Bouchy et al. (2010)
HAT-P-6b	0.05235	1278	1.33465	1.33457	1.32848	1.33000	1.33102	1.00464	0.194	1628	Noyes et al. (2008)
WASP-13b	0.05270	2937	1.21722	1.21711	1.20767	1.21000	1.21159	1.00791	0.231	1439	Skillen et al. (2009)
HAT-P-9b	0.05300	1718	1.40744	1.40731	1.39759	1.40000	1.40164	1.00705	0.223	1487	Shporer et al. (2009)
HAT-P-11b	0.05300	10473	0.45248	0.45248	0.45184	0.45200	0.45211	1.00142	0.130	844	Bakos et al. (2010)
SWEEPS-04	0.05500	341	0.81015	0.81014	0.80995	0.81000	0.81003	1.00024	0.073	1348	Sahu et al. (2006)
HAT-P-1b	0.05530	2264	1.23003	1.22996	1.22336	1.22500	1.22611	1.00545	0.205	1259	Bakos et al. (2007b)
XO-4b	0.05550	803	1.34252	1.34248	1.33917	1.34000	1.34055	1.00250	0.159	1414	McCullough et al. (2008)
CoRoT-3b	0.05700	66	1.01006	1.01006	1.00998	1.01000	1.01001	1.00008	0.052	1656	Deleuil et al. (2008)
HAT-P-14b	0.06060	650	1.15084	1.15083	1.14972	1.15000	1.15019	1.00098	0.116	1525	Torres et al. (2010)
WASP-7b	0.06180	1396	0.91568	0.91568	0.91477	0.91500	0.91515	1.00099	0.116	1344	Hellier et al. (2009)
Kepler-7b	0.06224	3258	1.48887	1.48871	1.47451	1.47800	1.48040	1.00974	0.248	1514	Latham et al. (2010)
HAT-P-2b	0.06878	156	1.15714	1.15714	1.15695	1.15700	1.15703	1.00016	0.065	1442	Pál et al. (2009)
WASP-8b	0.07930	485	1.17030	1.17030	1.16990	1.17000	1.17007	1.00034	0.082	912	Smith et al. (2009)
CoRoT-6b	0.08550	373	1.16618	1.16618	1.16594	1.16600	1.16604	1.00021	0.070	990	Fridlund et al. (2010)
CoRoT-4b	0.09000	1600	1.19072	1.19072	1.18976	1.19000	1.19016	1.00081	0.108	1039	Moutou et al. (2008)
HD 17156b	0.16230	404	1.02302	1.02302	1.02299	1.02300	1.02300	1.00002	0.033	852	Winn et al. (2009)
CoRoT-9b	0.40700	1234	1.05000	1.05000	1.05000	1.05000	1.05000	1.00000	0.019	401	Deeg et al. (2010)
HD 80606b	0.44900	239	0.92100	0.92100	0.92100	0.92100	0.92100	1.00000	0.009	365	Fossey et al. (2009)

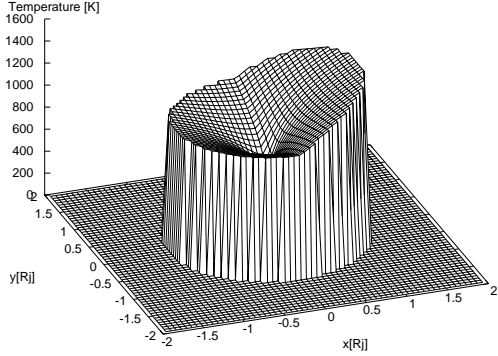


Fig. 1.— Example of a 2D projection map of the surface temperature of HD189733b calculated for  $P_r = 0.6$ ,  $P_a = 0.1$ . x-axis points to the star, z-axis to the rotation pole. One can clearly see the hot region on the day side of the planet facing the star. The night side has a non zero temperature due to the efficient heat redistribution ( $P_r = 0.6$ ). The temperature at the polar region,  $(x, y) = (0, 0)$ , drops significantly since the heat is redistributed efficiently along parallels but much less effectively along the meridians ( $P_a = 0.1$ ).

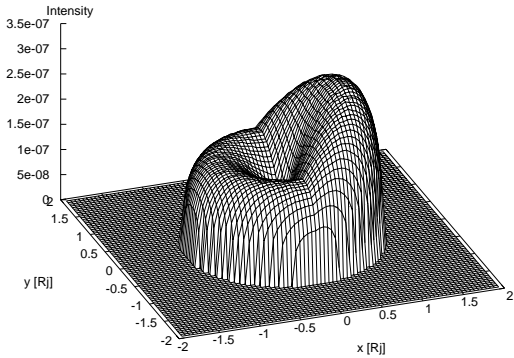


Fig. 2.— Example of a 2D projection image of HD189733b at 8 micron seen pole-on. The surface intensity is in  $\text{erg/s/Hz/cm}^2/\text{sterad}$ . It corresponds to the temperature distribution from Fig.1. The limb darkening ( $u_1 = 0.6$ ,  $u_2 = 0.2$ ) was applied to it. Notice that hot regions are now actually dark due to the limb darkening.

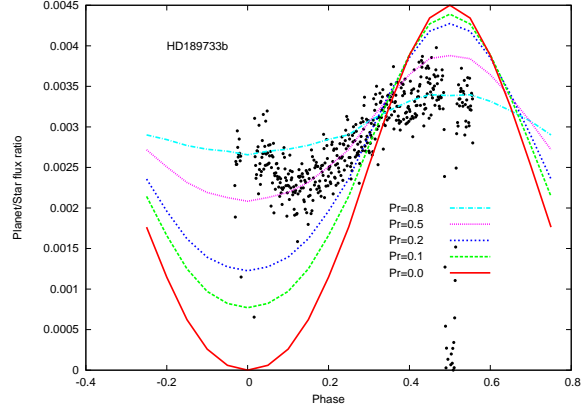


Fig. 3.— Theoretical light-curves of HD189733b compared with the observations of Knutson et al. (2007) at 8 micron (black points). Observe the strong dependence on the heat redistribution parameter,  $P_r$ , which could reach several orders of magnitude at phase zero.  $A_B = 0$ ,  $P_a = 1.0$ , and zero limb darkening were assumed.

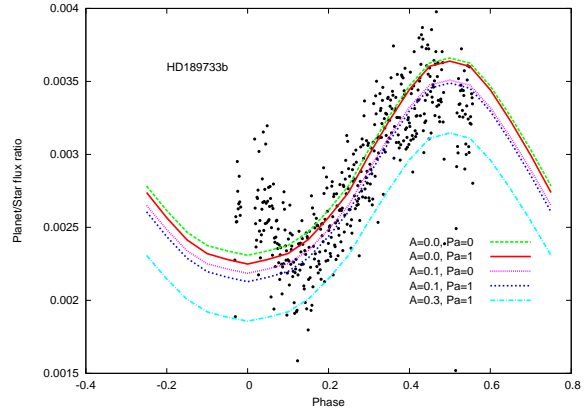


Fig. 4.— The effect of the Bond albedo and zonal temperature distribution on the light-curve of transiting exoplanet HD189733b at 8 micron. Higher Bond albedo reflects more light which is seen mainly at shorter wavelength. Consequently, less energy is available to be absorbed and redistributed over the surface. Temperatures are lower which means lower fluxes in the IR region. If  $P_a = 0$  and the heat flows mainly along the parallels then (compared to the homogeneous flows with  $P_a = 1$ ) one would detect slightly more light at all phases, especially on the night side. Black points are the observations of Knutson et al. (2007).  $P_r = 0.6$  and zero limb darkening were assumed.

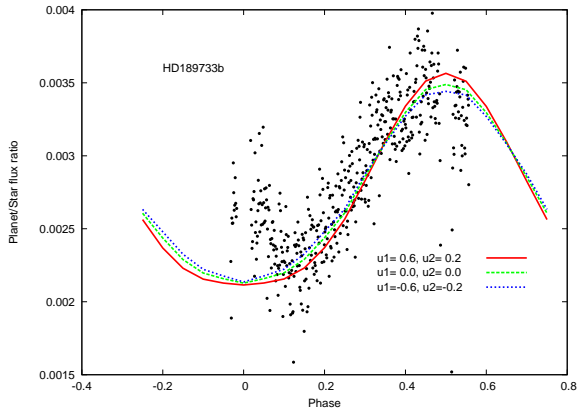


Fig. 5.— The effect of the limb darkening/brightening on the theoretical light-curve of the transiting exoplanet HD189733b at 8 micron. Limb darkening has almost no effect at phase zero but much stronger effect shortly before and after the transit and near the secondary eclipse. This is because when we observe the night side with almost constant temperature distribution the darkening at the limb is compensated by the brightening at the center to conserve the flux. However, during the secondary eclipse the limb darkening suppresses the radiation from the cold regions and amplifies the radiation from the hot regions. The net effect is that planet is brighter at the phase 0.5. The opposite happens shortly before and after the transit. The possible limb brightening would have the opposite behaviour. Black points are the observations of Knutson et al. (2007).  $A_B = 0.1, P_r = 0.6, P_a = 1.0$  were assumed.

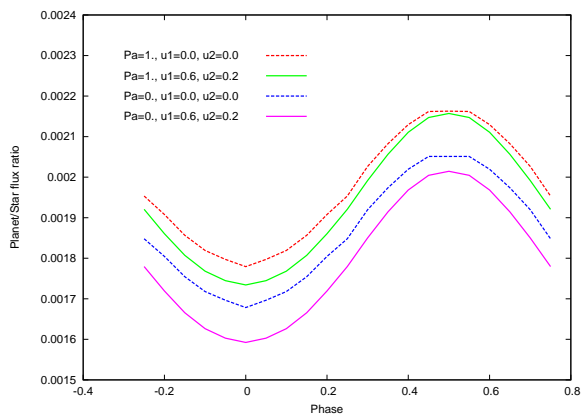


Fig. 6.— The effect of the zonal temperature redistribution ( $P_a$  parameter) and limb darkening on the light-curve of a hypothetical exoplanet seen at small inclination of 20 degrees. Contrary to the case with homogeneous temperature distribution ( $P_a = 1$ ), one would observe less flux from the models with the dominant east-west heat circulation ( $P_a = 0$ ) since the polar regions visible at this inclination are quite cool. Limb darkening would dim the hotter equatorial regions even further and reduce the observed flux, especially for models with the dominant east-west heat circulation ( $P_a = 0$ ).  $A_B = 0, P_r = 0.5$  were assumed.

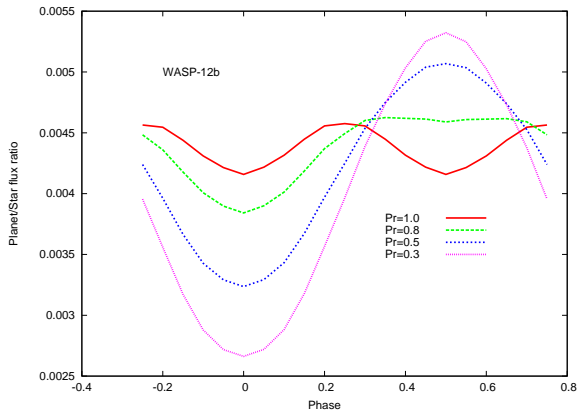


Fig. 7.— Illustration of the effect of the non-spherical shape on the light-curve of WASP-12b at 8 microns. In case of effective heat redistribution ( $P_r = 1$ ), one would observe a highly atypical double humped light-curve caused by the Roche shape. This resembles the well known ellipsoidal variations in interacting binaries. For lower values of  $P_r$  and less effective heat redistribution the light curve would acquire a more typical 'cosine' shape.  $A_B = 0, P_a = 1$  and zero limb darkening were assumed.

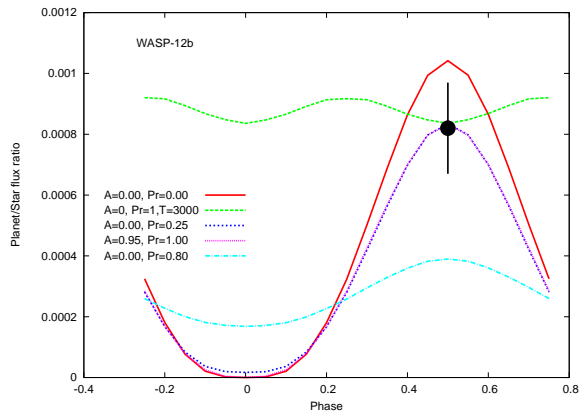


Fig. 8.— Light-curves of WASP-12b at 0.9 microns. Observations of Lopez-Morales et al. (2009), black point, can be understood within several very different models. Low albedo and low heat redistribution model ( $A_B = 0, P_r = 0.25$ ) produces almost identical light-curve than high albedo models ( $A_B = 0.95, P_r$  is not very important in this case). Also a non-reflective model with homogeneous temperature distribution of about 3000 K ( $A_B = 0, P_r = 1, P_a = 1$ ) can reproduce the observations. Roche shape and zero limb darkening were assumed.

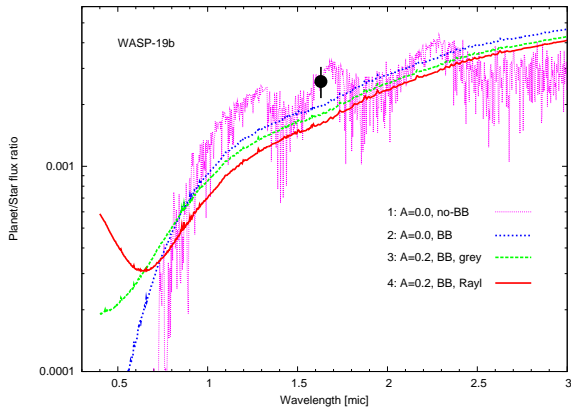


Fig. 9.— Planet to star flux ratio as a function of wavelength for WASP-19b. Model (2) is a black-body model with zero albedo. Model (3) is a grey albedo model ( $A_B = 0.2$ ). Model (4) is a non-grey albedo model (Rayleigh scattering) and the same Bond albedo,  $A_B = 0.2$ . Model (1) is a non black-body model based on non-irradiated atmospheres (Hubeny & Burrows 2007; Allard et al. 2003). Black symbol is a measurement of Anderson et al. (2010b) in the H-band. Zero heat and homogeneous zonal temperature redistribution ( $P_r = 0, P_a = 1$ ) and zero limb darkening were assumed.